

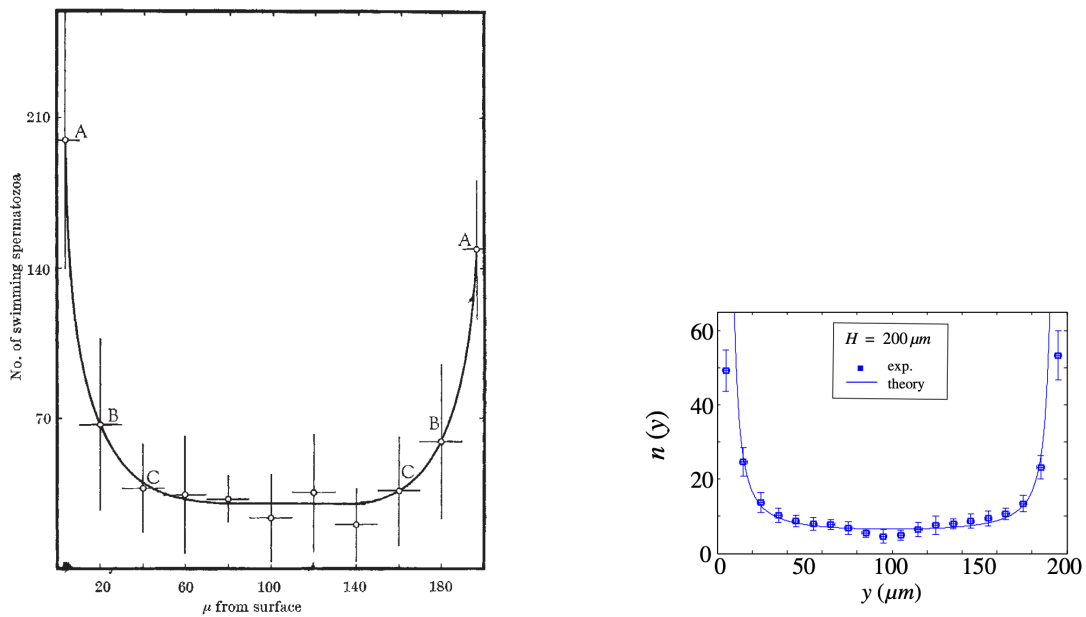
Brownian Microswimmers: Investigating models  
that capture boundary accumulation of  
microorganisms

Inti-Raymi Carhuancho Mantripp

Candidate Number: 1090497

# 1 Introduction

Many types of self-propelled microorganisms moving through water tend to accumulate near the boundaries of their environments. This has been observed both experimentally, [1], [2] and in nature. Figure 1 shows two characteristic illustrations of this behaviour by plotting the density cells and bacteria observed cross-sectionally within their domains.



(a) Distribution of bull spermatozoa in suspended medium [1].

(b) Distribution of E. coli bacteria between two glass plate [2].

Figure 1: Experimental results illustrating boundary accumulation of swimming microorganisms.

Many models have been proposed to describe the behaviour of microswimmers([3], [2], [4]), and this observed boundary accumulation is an important feature for such models to capture. The purpose of such models is not only to describe this behaviour but also to provide some explanation behind it.

The goal of this report is to present three models that describe the behaviour of swimming microorganisms, with a particular focus on capturing the observed boundary accumulation. Before introducing these models, a brief overview of stochastic PDEs and the Fokker-Planck equation will be given.

The structure of this report is as follows:

## 2 Main

The dynamics of microorganisms are in part the result of microscopic interactions between organisms and their surrounding environment SOURCE NEEDED. Rather than model this directly, this is typically captured by introducing stochastic terms to their dynamics. This is done in all the models covered in this report, and for that reason we will give an overview of stochastic differential equations (SDEs) followed by their solution via the Monte Carlo methods and the Fokker-Planck equation.

### 2.1 Stochastic Differential Equations and the Fokker-Planck Equation

For the purposes of this report, SDEs can be conceptually viewed as differential equations with an additional random term that introduces stochastic fluctuations to their dynamics.

To illustrate, consider the deterministic differential equation:

$$dx = \mu(x(t), t)dt.$$

Here,  $x(t)$  is a deterministic variable with a drift term  $\mu(x(t), t)$ , mapping  $\mathbb{R} \times [0, \infty) \rightarrow \mathbb{R}$ . By adding stochasticity through Brownian motion

$$dX = \mu(X(t), t)dt + \sigma(X(t), t)dW \quad (1)$$

where  $X(t)$  is now a stochastic process. Here,  $\mu(X(t), t)dt$  continues to be the deterministic drift term, while  $\sigma(X_t, t)$  is known as the *diffusion term*, scaling the stochastic fluctuations introduced by the Wiener process  $W_t$ . The increments of  $W_t$  are normally distributed as follows:

$$dW \sim \mathcal{N}(0, dt).$$

By selecting a sufficiently small time step  $\Delta t$ , we discretise equation (1) to numerically approximate the differential as:

$$\Delta X = \mu(X(t), t)\Delta t + \sigma(X(t), t)\Delta W \quad (2)$$

Equation (2) can be used in an iterative approach to obtain a sample trajectory of the SDE in equation (1):

$$X(t + \Delta t) = X(t) + \Delta X. \quad (3)$$

This method is called the Euler-Maruyama method, a stochastic analogue of the forward Euler method [5].

As  $X(t)$  is a stochastic process, at any fixed time  $t$ ,  $X(t)$  has a distribution described by its probability distribution function (PDF). To obtain the PDF of the random variable  $X(t)$  at a given time  $t$ , two main approaches exist. Firstly, using the Euler-Maruyama method one can generate  $n$  independent trajectories of the SDE. Provided  $n$  is sufficiently large, one can construct an empirical density from the realisations of  $X(t)$  at time  $t$ . This approach is called the Monte Carlo method, and its accuracy depends on the number of samples  $n$ . By the central limit theorem, the error in estimating the PDF decreases like:

$$\text{Error} \sim \mathcal{O}(n^{-1/2}).$$

This means that to halve the error we must quadruple the number of samples. This can make Monte Carlo methods computationally expensive for high precision estimates.

An alternative approach to determining the PDF is through the Fokker-Planck equation. The Fokker-Planck equatino is a partial differential equation (PDE) describing the evolution of the PDF  $p(x, t)$  associated with  $X(t)$ . For the SDE given in equation (1), the corresponding Fokker-Planck equation is:

$$\frac{\partial p(x, t)}{\partial t} = -\frac{\partial}{\partial x} [\mu(x, t)p(x, t)] + \frac{1}{2} \frac{\partial^2}{\partial x^2} [\sigma^2(x, t)p(x, t)], \quad (4)$$

where  $p(x, t)$  is the probability density function of the random variable  $X_t$ . Solving this PDE can directly yield the PDF without the sampling noise inherent in Monte Carlo simulations.

For systems involving multiple interacting stochastic processes, we consider a system of coupled SDEs:

$$d\mathbf{X}_t = \boldsymbol{\mu}(\mathbf{X}_t, t), dt + \boldsymbol{\Sigma}(\mathbf{X}_t, t), d\mathbf{W}_t, \quad (5)$$

where  $\mathbf{X}_t \in \mathbb{R}^n$  is a vector-valued stochastic process,  $\boldsymbol{\mu}(\mathbf{X}_t, t)$  is a vector of drift terms,  $\boldsymbol{\Sigma}(\mathbf{X}_t, t)$  is a diffusion matrix, and  $\mathbf{W}_t \in \mathbb{R}^m$  is a vector of independent Wiener processes. The associated Fokker-Planck equation describing the evolution of the joint probability density  $p(\mathbf{x}, t)$  for the system is given by:

$$\frac{\partial p(\mathbf{x}, t)}{\partial t} = -\nabla_{\mathbf{x}} \cdot [\boldsymbol{\mu}(\mathbf{x}, t)p(\mathbf{x}, t)] + \frac{1}{2}\nabla_{\mathbf{x}} \cdot (\nabla_{\mathbf{x}} \cdot [\boldsymbol{\Sigma}(\mathbf{x}, t)\boldsymbol{\Sigma}(\mathbf{x}, t)^T p(\mathbf{x}, t)]) . \quad (6)$$

where  $\nabla_{\mathbf{x}}$  is the gradient operator with respect to the spatial variables  $\mathbf{x}$ . Solving this PDE provides a direct method for obtaining the joint probability distributions of systems of interacting stochastic systems.

## 2.2 Model 1: Pure Stochastic Model

The first model we present considers an elliptic cell with orientation  $\theta$  placed within a channel of infinite width and fixed height  $H$ . The setup for this model is illustrated in Figure 2.

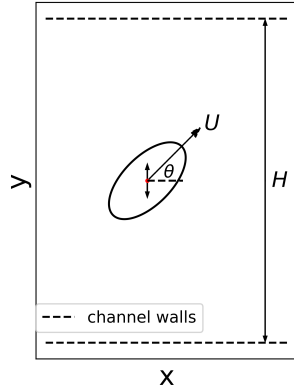


Figure 2: An elliptic cell with orientation  $\theta$  located within a channel of fixed height  $H$  and infinite width. The channel walls are considered reflective boundaries.

The dynamics imposed on the cell are described by the following coupled SDEs:

$$Y(t + \Delta t) = Y(t) + U \sin(\theta) + \sqrt{2D_y} \Delta W_1 \quad (7a)$$

$$\theta(t + \Delta t) = \theta(t) + \sqrt{2D_\theta} \Delta W_2 \quad (7b)$$

Here,  $Y(t)$  denotes the vertical position of the cell's geometric centre at time  $t$ , and  $\theta$  its orientation at that time. The parameters  $D_y$  and  $D_\theta$  scale the respective Brownian motion terms, modelling random fluctuations in position and orientation. The parameter  $U$  sets the deterministic speed of the cell's motion along the  $y$ -axis, thereby controlling the magnitude of the directed movement within the channel. We treat the upper and lower channel walls as reflective boundaries. Movement along

the  $x$ -axis is disregarded, as our primary interest is in understanding whether this system exhibits boundary accumulation behaviour. Given the channel's infinite extent along the  $x$ -axis, horizontal movements have no meaningful impact on the boundary accumulation analysis. care primarily about whether this system exhibits boundary accumulating behaviour. With no bounds along  $x$ , it is irrelevant to consider movement along the  $x$ -axis.

Our primary objective is to identify whether this system exhibits boundary accumulation behaviour. To investigate this, we seek the stationary distribution - the long-term PDF to which the system converges as  $t \rightarrow \infty$ . To obtain this stationary distribution, two approaches are available: Performing Monte Carlo simulations using equations (7), or directly solving the corresponding Fokker-Planck PDE.

Both of these approaches however first require us to identify the configuration space of the system - the space of possible configurations of  $y$  and  $\theta$  the system can inhabit. As the cell's orientation  $\theta$  is periodic and thus unbounded, the vertical position  $y$  is constrained by the channel walls. Specifically, the minimum distance the centre of the clel can approach each channel wall depends explicitly on its orientation  $\theta$ . This dependency is illustrated in Figure 3.

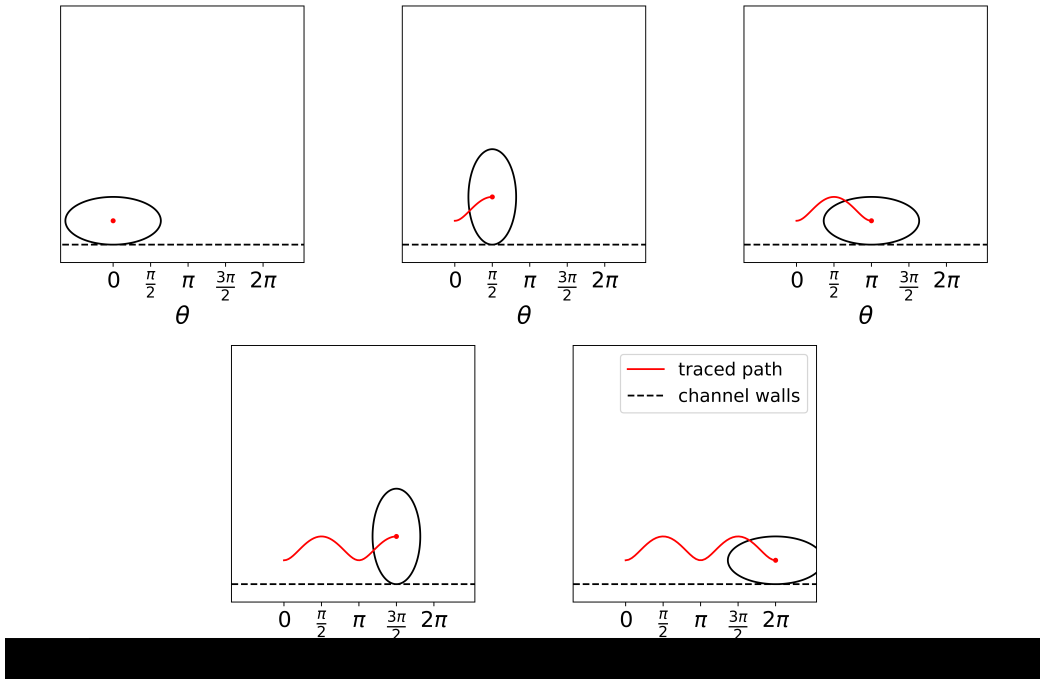


Figure 3: Path traced by the oval's centre, illustrating the minimum distance achievable to a horizontal wall as a function of orientation  $\theta$

The function characterising this minimum distance is termed the *wall distance*

function [3]. For the specific case of an ellipse, this function is defined by:

$$y_{min}(\theta) = \sqrt{a^2 \sin^2(\theta) + b^2 \cos^2(\theta)} \quad (8a)$$

$$y_{max}(\theta) = H - \sqrt{a^2 \sin^2(\theta) + b^2 \cos^2(\theta)} \quad (8b)$$

where  $a$  and  $b$  are the major and minor semi-axes for the elliptic cell, respectively. Equations (8) establish the upper and lower boundaries of the configuration space for this system. Figure 4 illustrates the derived configuration space.

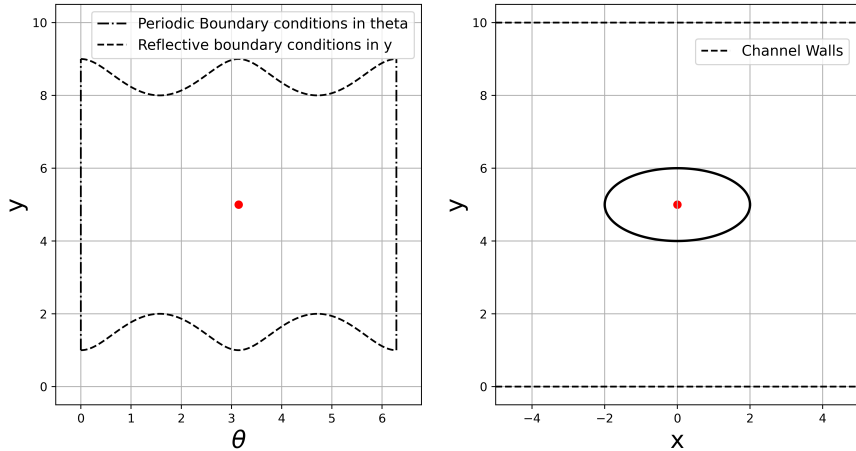


Figure 4: Configuration space for Model 1 and its correspondance to the physical system of a cell within a channel. Parameters used:  $a = 2$ ,  $b = 1$ ,  $H = 10$

Figure 4 also shows the boundary conditions applied to the configuration space. Periodic boundary conditions on the orientation variable  $\theta$  at  $\theta = 0$  and  $\theta = 2\pi$ , while reflective boundary conditions are applied at the upper and lower boundaries described by  $y_{min}(x)$  and  $y_{max}(x)$ .

With a clearly bounded configuration space, the corresponding Fokker-Planck equation associated with equations (7) can be solved. The corresponding Fokker-Planck equation is:

$$\frac{\partial p}{\partial t} = -\frac{\partial}{\partial y}(U \sin(\theta)p) + D_\theta \frac{\partial^2 p}{\partial \theta^2} + D_y \frac{\partial^2 p}{\partial y^2} \quad (9)$$

When solving equation (9), no-flux boundary conditions are applied at the upper and lower boundaries along the  $y$ -axis, accounting for the conservation of probability within the domain. The finite element solver COMSOL Multiphysics® was used to

numerically obtain the stationary distribution [6]. The resulting PDF is presented in Figure 5a, and the resulting marginal distribution across the channel is displayed in Figure 5b.

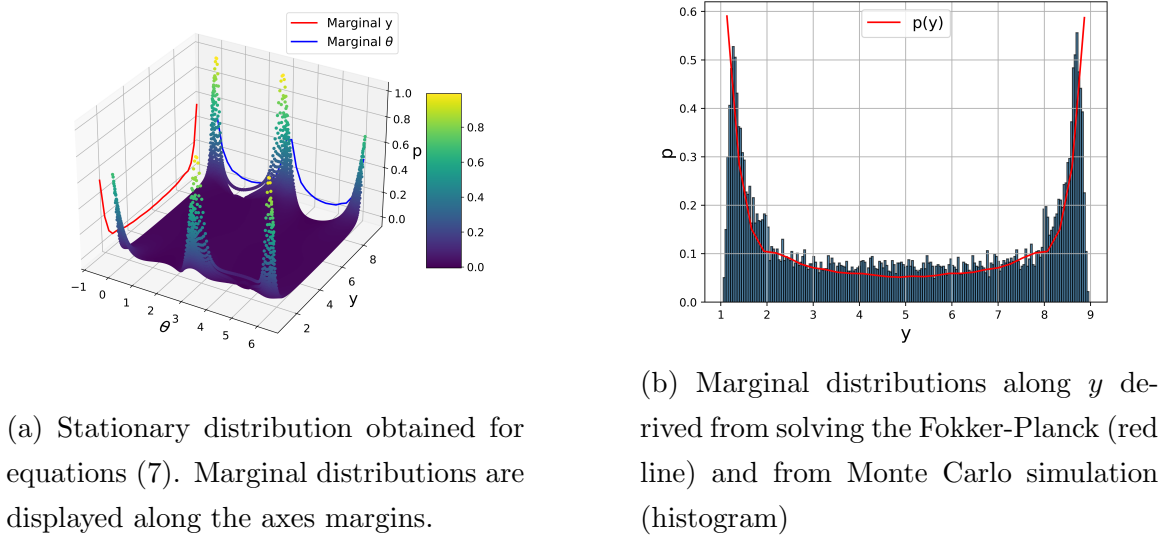


Figure 5: Comparison of stationary distribution and its marginal along  $y$ .

The marginal distribution along the  $y$ -axis clearly exhibits characteristic boundary accumulation behaviour. We attribute this phenomenon as arising from two primary mechanisms. Firstly, the drift term in equation (7a) implies that, on average, the cell moves towards and eventually encounters the boundary, where it becomes constrained until it sufficiently reorients. Secondly, the geometry of the configuration space contributes significantly; the elliptical shape introduces two "hills" with reflective boundaries. These features act as barriers, hindering the ease with which the system can exit the boundary regions, thus enhancing the boundary accumulation.

### 2.3 Model 2: Hydrodynamics Informed Model

The second model examined was introduced by Chen et al. [3], building on the prior work of Spagnolie et al. [7]. This model extends the previous analysis by explicitly incorporating hydrodynamic interactions between the channel walls into the governing SDEs.

Spagnolie et al. approximate the velocity field surrounding an elliptical microswimmer by treating it first as a *stresslet* - a force dipole - and then applying Faxén's Law to derive the corresponding velocity field associated with an elliptical

stresslet. Figures 6 illustrates the microswimmer as a stresslet and the velocity field generated by such an elliptical swimmer, near a circular boundary.

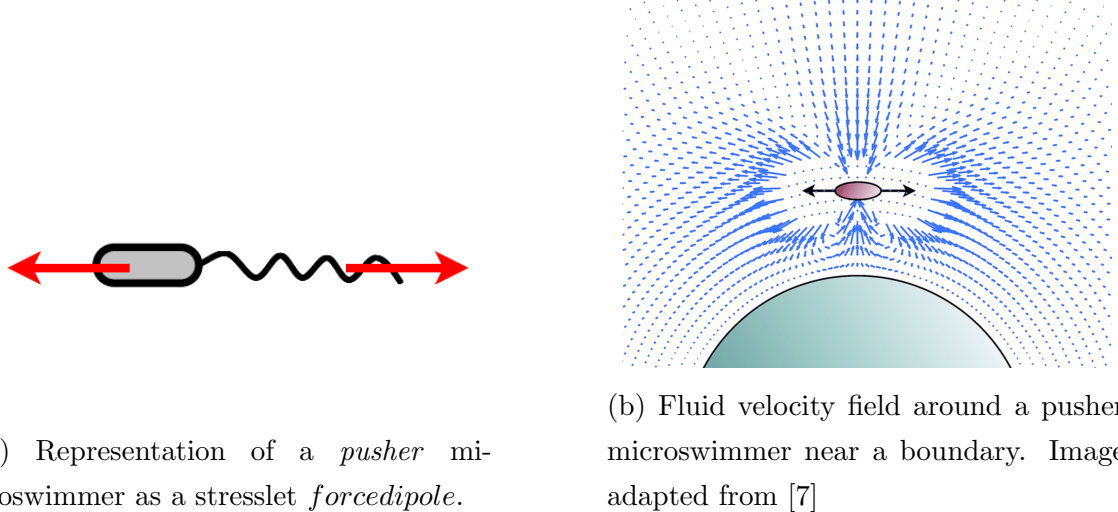


Figure 6: Visual depiction of key components in hydrodynamic model.

Microswimmers are commonly classified as either *pushers* or *pullers*, based on whether they propel themselves by pushing fluid back or pulling fluid forward [2]. In this analysis we consider solely pusher-type microswimmers.

Spagnolie et al. derived hydrodynamic equations describing the boundary-induced effects on the cell's motion near a circular boundary:

$$\frac{dr}{dt} = \sin(\theta) - \frac{3\alpha}{8r^2}(1 - 3\sin^2(\theta)) \quad (10a)$$

$$\frac{d\theta}{dt} = \frac{1}{A} - \frac{3\alpha}{64r^3}[4 - \Gamma(3 - \cos(2\theta))] \sin(2\theta) \quad (10b)$$

where  $\alpha$  denotes the dipole strength, with  $\alpha > 0$  for pushers and  $\alpha < 0$  for pullers [2],  $\Gamma$  is the aspect ratio of the elliptical microswimmer,  $A$  is the radius of the circular boundary and  $r$  is the distance from this boundary.

For the scenario considered in this report - an elliptical swimmer within an infinite channel bounded above and below by parallel walls - we take the limit as  $A \rightarrow \infty$ . In this limit, we define the vertical distance  $y$  from the cell centre to the channel walls along the  $y$ -axis. The resulting modified equations are given by Chen et al. [3] as:

$$\frac{dy}{dt} = \sin(\theta) - \frac{3\alpha}{8h^2} \left( \frac{a^2}{y^2} - \frac{a^2}{(H-y)^2} \right) (1 - 3 \sin^2(\theta)) \quad (11a)$$

$$\frac{d\theta}{dt} = -\frac{3\alpha}{64y^3} \left( \frac{a^3}{y^3} + \frac{a^3}{(H-y)^3} \right) [4 - \Gamma(3 - \cos(2\theta))] \sin(2\theta). \quad (11b)$$

Where  $H$  is the fixed channel height.

Incorporating equations (11) into the stochastic framework established in model 1 (7), we obtain the following system of SDEs describing the swimmers dynamics:

$$Y(t + \Delta t) = Y(t) + U \sin(\theta) \Delta t - \frac{3U\alpha}{8} \left( \frac{a^2}{y^2} - \frac{a^2}{(H-y)^2} \right) (1 - 3 \sin^2(\theta)) \Delta t + \sqrt{2D_y} \Delta W_1 \quad (12a)$$

$$\theta(t + \Delta t) = \theta(t) - \frac{3U\alpha}{64\alpha} \left( \frac{a^3}{y^3} + \frac{a^3}{(H-y)^3} \right) [4 - \Gamma(3 - \cos(2\theta))] \sin(2\theta) \Delta t + \sqrt{2D_\theta} \Delta W_2 \quad (12b)$$

Monte-Carlo simulations were performed to obtain the stationary marginal distributions associated with (12). These distributions are presented in Figure 7.

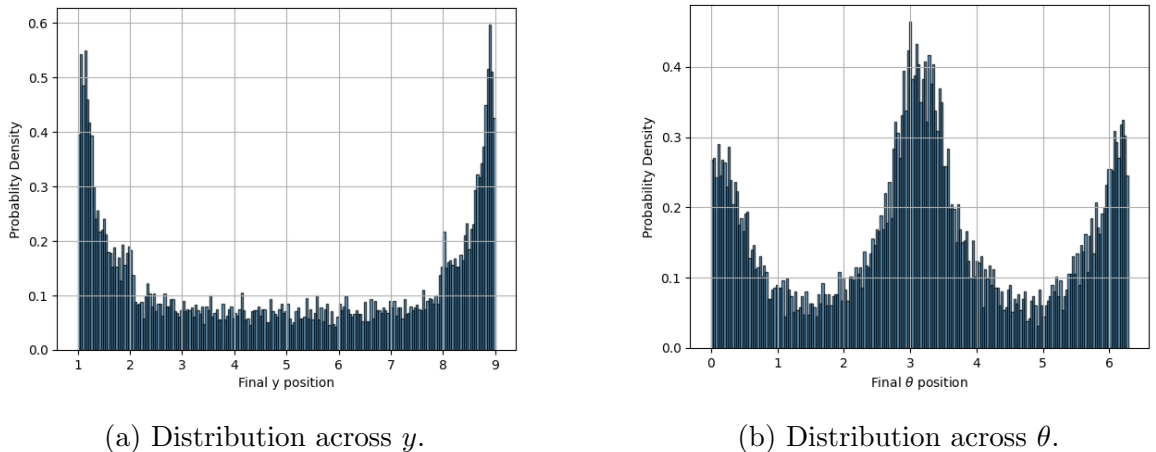


Figure 7: Marginal distributions obtained via Monte Carlo simulation from equations (12)

It can be observed that the same characteristic accumulation at the boundaries is obtained in the  $y$  distribution. Additionally, the angular distribution exhibits notable peaks at  $0$ ,  $\pi$ , and  $2\pi$ . This corresponds to cases where the cell is aligned parallel to the channel walls, highlighting a preferred orientation arising from hydrodynamic interactions.

## 2.4 Model 3: Bulk and Boundary Model

The third model considered is proposed by Fu et al. [8]. They propose a simplified model that explicitly incorporates boundary accumulation. Stochasticity is only present in the angular variable  $\theta$ , and there is no shape or hydrodynamic forces incorporated, so only a point particle is considered.

The model imposes boundary accumulation by introducing a free-swimming phase (FSP) and two boundary capture phases, corresponding to interactions with the upper and lower channel walls. In the free-swimming phase, the cell swims at a constant speed  $U$  while experiencing stochasticity solely in its angular orientation. Upon contact with either boundary, the cell transitions to a boundary-capture phase (BCP), remaining stationary at the boundary until its orientation changes sufficiently - due to continued rotational Brownian motion - to direct its trajectory away from the wall.

The SDEs describing this system are:

$$Y(t + \Delta t) = \begin{cases} Y(t) + U \sin(\theta) \Delta t, & \text{if } |Y(t)| \leq \frac{H}{2} \text{ or } |Y(t)| = \frac{H}{2} \text{ and } Y(t)\theta(t) \leq 0 \\ Y(t), & \text{if } |Y(t)| = \frac{H}{2} \text{ and } Y(t)\theta(t) \geq 0 \end{cases} \quad (13a)$$

$$\theta(t + \Delta t) = \theta(t) + \sqrt{2D_\theta} dW. \quad (13b)$$

In this model, the vertical coordinate system is centred such that  $y = 0$  corresponds to the midpoint of the channel, with channel boundaries positioned at  $y = \frac{H}{2}$  and  $y = -\frac{H}{2}$ . Additionally,  $\theta$  now ranges between  $[-\pi, \pi]$ . This choice of coordinates simplifies the conditional statements in equations (13). An illustration of the model is shown in Figure 8.

The authors propose the following Fokker-Planck system for SDEs (13). These equations are degenerate, as the particles motion in  $y$  is deterministic.

$$\frac{\partial p}{\partial t} + U \sin(\theta) \frac{\partial p}{\partial y} - D_\theta \frac{\partial^2 p}{\partial \theta^2}, \quad (y, \theta) \in \Omega \quad (14a)$$

$$\frac{\partial p_+}{\partial t} - D_\theta \frac{\partial^2 p_+}{\partial \theta^2} = U \sin(\theta) p(t, \frac{H}{2}, \theta), \quad (\frac{H}{2}, \theta), \quad (\frac{H}{2}, \theta) \in \Omega_+ \quad (14b)$$

$$\frac{\partial p_-}{\partial t} - D_\theta \frac{\partial^2 p_-}{\partial \theta^2} = -U \sin(\theta) p(t, -\frac{H}{2}, \theta), \quad (-\frac{H}{2}, \theta), \quad (-\frac{H}{2}, \theta) \in \Omega_+ \quad (14c)$$

where  $p(t, y, \theta)$  is the PDF of the cells in the FSP at time  $t$ , position  $y$  with orientation  $\theta$ , while  $p_{\pm}$  are the PDFs of boundary contacting cells at time  $t$ , position

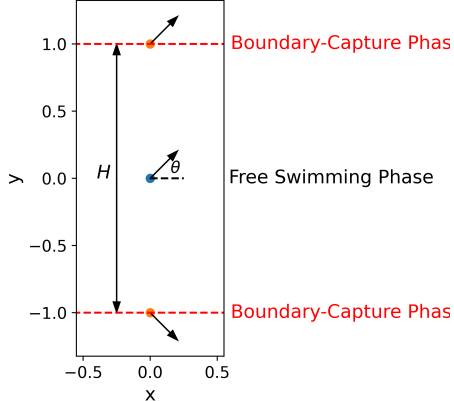


Figure 8: Schematic illustration of the system configuration for Model 3. Microswimmer is treated as a point particle in a channel of height  $H = 2$ , with boundaries at  $y = \frac{H}{2}$  and  $y = -\frac{H}{2}$ . The particle remains trapped at a boundary until its orientation is redirected inward, away from the boundary.

$\pm\frac{H}{2}$  with non-inward facing orientation.  $\Omega$  denotes the domain occupied by cells in FSP, while  $\Omega_{\pm}$  is the domains of the upper and lower BCPs, respectively.

The associated boundary conditions for (14) are as follows. First we consider the boundary conditions associated with cells in the FSP (14a). As cells with direction  $\theta = \pi$  and  $\theta = -\pi$  are the same, we have periodic boundary conditions in  $\theta$ :

$$p(t, y, -\pi) = p(t, y, \pi), \quad \frac{\partial p}{\partial \theta}(t, y, -\pi) = \frac{\partial p}{\partial \theta}, \quad -\frac{H}{2} < y < \frac{H}{2} \quad (15)$$

Further, as it is impossible for cells in the BCP with outward-facing orientation to enter the FSP, we impose Dirichlet boundary conditions at the channel walls:

$$p(t, L, \theta) = 0, \quad \theta \in (-\pi, 0), \quad p(t, -L, \theta) = 0, \quad \theta \in (0, \pi). \quad (16)$$

For cells in the BCP described by (14b), (14c), the cells exit this phase once their orientation points inward, resulting in Dirichlet boundaries in BCP at  $\theta = 0, \theta = \pm\pi$ :

$$p_+(t, 0) = p_+(t, \pi) = 0, \quad p_-(t, 0) = p_-(t, -\pi) = 0. \quad (17)$$

Transitions between phases are characterised by source and sink terms, which represent probability fluxes between the BCP and FSP. These fluxes are described by the following conditions:

$$\frac{\partial p}{\partial \theta}(t, y, \theta) \Big|_{\theta=\pi_-}^{\theta=\pi_+} = \frac{\partial p_+}{\partial \theta}(t, \pi_-) \delta_{y=\frac{H}{2}} - \frac{\partial p_-}{\partial \theta}(t, \pi_+) \delta_{y=-\frac{H}{2}} \quad (18a)$$

$$\frac{\partial p}{\partial \theta}(t, y, \theta) \Big|_{\theta=0_-}^{\theta=0_+} = -\frac{\partial p_+}{\partial \theta}(t, 0_+) \delta_{y=\frac{H}{2}} + \frac{\partial p_-}{\partial \theta}(t, 0_-) \delta_{y=-\frac{H}{2}} \quad (18b)$$

The convergece of this system is analysed by Fu et al. [8], and solved via a finite difference scheme on a stencil depicted in Figure 9.

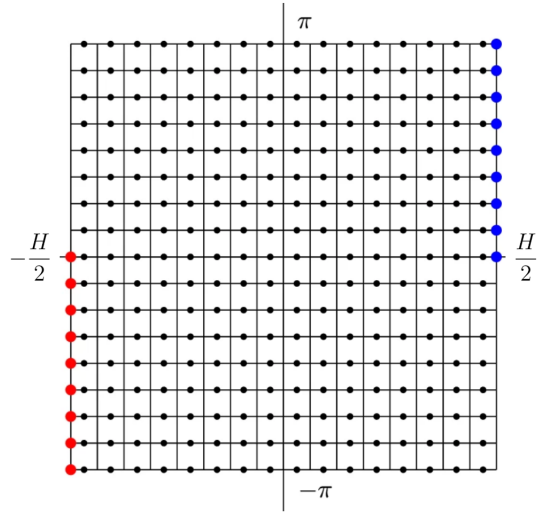
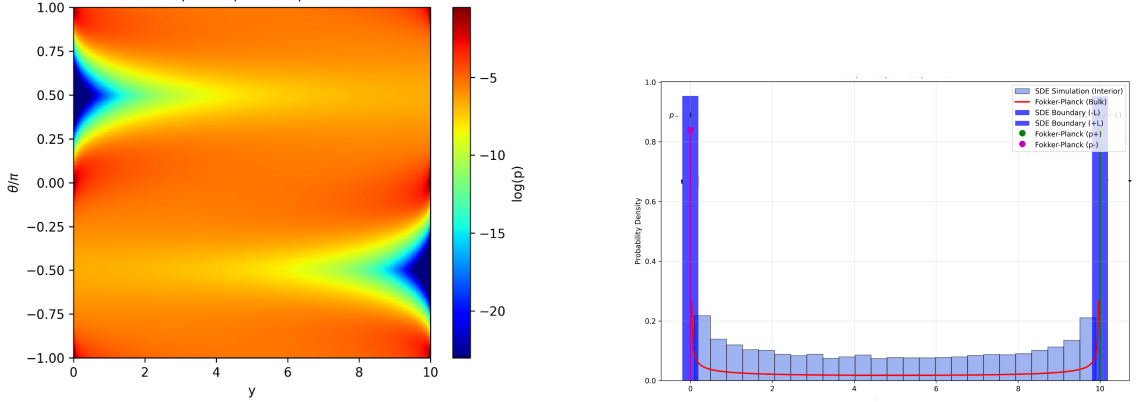


Figure 9: Stencil of finite difference scheme implemented to obtain stationary distribution for (14). Red dots correspond to nodes in the lower BCP, blue dots correspond to nodes in the upper BCP.

We employed both the finite-difference scheme and Monte Carlo simulations to obtain the stationary distribution corresopnding to equations (14). The resulting PDF and marginal distribution is presented in 10.

Figure 10b demonstrates the characteristic boundary accumulation, which is expected given that boundary accumulation is explicitly built into this model. Additionally, Figure 10a exhibits regions of extremely low probability density in the upper-left



(a) Heatmap of stationary distribution obtained from (14). Parameters are:  $H = 10$ ,  $U = 25$ ,  $D_\theta = 0.5$ .

(b) Marginal distribution along the channel obtained by Monte Carlo (histogram) and finite-difference scheme (solid lines).

Figure 10: Stationary and marginal distributions for the system described by equations (14).

and lower-right corners. These correspond to regions where the cell’s motion is directed opposite to its vertical orientation, making such configurations highly unlikely. The probability is 0 in these regions directly against the boundary, as it is impossible for the cell to exit the BCP while its orientation is against the opposite channel.

## 2.5 Modifying Model 3 & Comparison of Models

In Model 3, the cell was treated as a point particle, neglecting the effects of cell shape on boundary interactions. To address this limitation, we explored incorporating cell geometry explicitly into Model 3, aiming to understand how the resulting PDF would compare to the shape0-dependent outcomes observed in Models 1 and 2.

This integration of shape could be implemented through multiple approaches. Our chosen method involved redistributing the probability mass from the boundary accumulation peaks observed in the marginal distribution along  $y$  (see Figure 10b) over a finite region corresponding to the physical contact of an elliptical cell with the channel walls. Specifically, we computed the geometric average distance of an elliptically shaped cell from the wall and redistributed the probability previously representing point-particle capture in Model 3, were distributed. The computed average boundary distance for an ellipse is illustrated by the solid red line in Figure 11.

The average was calculated as  $\bar{y} = \frac{1}{2\pi} \int_0^{2\pi} \sqrt{a^2 \sin^2(\theta) + b^2 \cos^2(\theta)}$ , where the in-

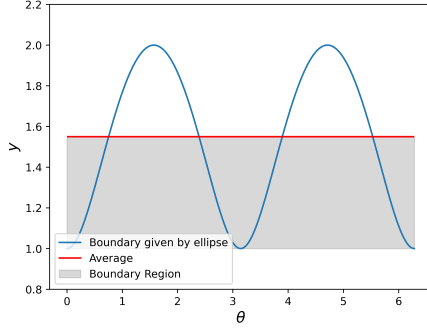


Figure 11: Illustration of methodology for redistributing boundary-accumulated probability mass based on the geometric average boundary distance of an elliptical cell.

tegrand corresponds to the wall distance function previously defined in (8). The resulting adjusted marginal distribution is given in Figure 12.

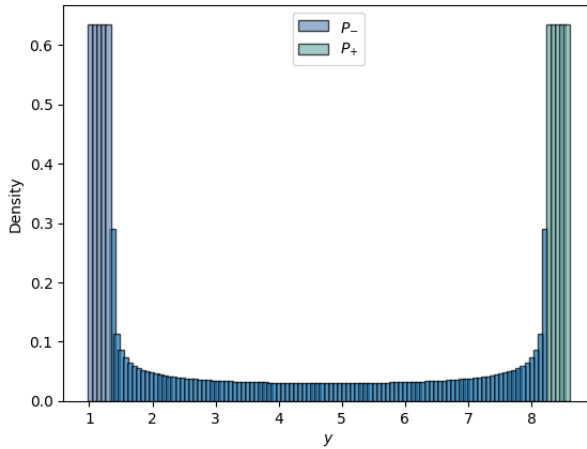


Figure 12: Marginal distribution after redistributing Model 3's boundary-accumulated probability mass according to the cell shape.

Finally, we compared the marginal distributions from Model 1, Model 2 and the modified version of Model 3. These distributions, generated with identical parameters for consistency, are shown in Figure 13.

From Figure 13, Models 1 and 2 show close alignment, suggesting that additional hydrodynamic terms in Model 2 may have a relatively minor effect on boundary accumulation under the conditions investigated here. Further investigation through additional simulations and parameter variations is recommended to comprehensively understand the conditions under which hydrodynamic interactions significantly influence the observed cell behavior.

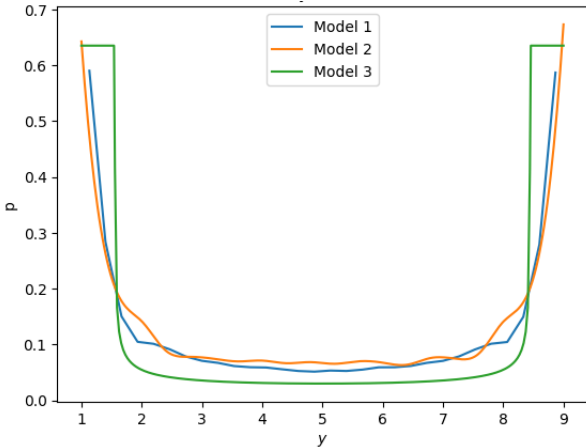


Figure 13: Comparison of Marginal PDFs from Model 1, Model 2, and the shape-adjusted Model 3.

In contrast, Model 3 assigns more probability mass at the boundaries compared to Models 1 and 2. This discrepancy suggests that the simplistic boundary interactions in Model 3 may overestimate the boundary accumulation effect.

For future work, several extensions can be considered:

- Investigate imposing Robin boundary conditions to more accurately capture interactions between cells and boundaries.
- Adjusting the cell's centre of rotation, which may substantially influence boundary accumulation phenomena, as is exposed in [3].
- Investigating the effects of alternative cell shapes beyond ellipses to generalise the results
- Exploring boundary accumulation behaviour near complex boundaries or obstacles, such as circular or irregular shapes within the channel.
- Considering collective interactions among the multiple cells to understand how inter-cellular dynamics affect boundary accumulation.

### 3 Conclusion

In this report, we investigated several stochastic models aiming to capture the boundary-accumulation behavior commonly observed in swimming microorganisms. We ana-

lyzed three distinct modeling approaches: a purely diffusive model, a model incorporating hydrodynamic interactions with the channel walls, and a piecewise-deterministic Markov process (PDMP) model that explicitly describes boundary capture.

Models 1 and 2, both accounting for cell geometry, provided closely aligned marginal distributions, suggesting that hydrodynamic interactions may exert a relatively minor influence under the conditions studied here. However, additional exploration of parameter spaces and physical scenarios remains essential to thoroughly quantify the role of hydrodynamics in these contexts.

In contrast, Model 3 initially treated cells as point particles, yielding exaggerated boundary accumulation. Incorporating geometric considerations into Model 3 led to a more realistic redistribution of boundary probabilities, yet notable differences remained compared to Models 1 and 2. This highlights the importance of accounting explicitly for cell geometry in accurately modeling boundary interactions.

## References

- [1] Rothschild. “Non-random distribution of bull spermatozoa in a drop of sperm suspension”. In: *Nature* 198.4886 (1963), pp. 1221–1222.
- [2] Allison P Berke et al. “Hydrodynamic attraction of swimming microorganisms by surfaces”. In: *Physical Review Letters* 101.3 (2008), p. 038102.
- [3] Hongfei Chen and Jean-Luc Thiffeault. “Shape matters: a Brownian microswimmer in a channel”. In: *Journal of Fluid Mechanics* 916 (2021), A15.
- [4] Bao-quan Ai et al. “Rectification and diffusion of self-propelled particles in a two-dimensional corrugated channel”. In: *Physical Review E* 88.6 (2013), p. 062129.
- [5] Radek Erban and S Jonathan Chapman. *Stochastic modelling of reaction–diffusion processes*. Vol. 60. Cambridge University Press, 2020.
- [6] COMSOL AB. *COMSOL Multiphysics® v6.3*. Available: <https://www.comsol.com>. Stockholm, Sweden, 2024.
- [7] Saverio E Spagnolie et al. “Geometric capture and escape of a microswimmer colliding with an obstacle”. In: *Soft Matter* 11.17 (2015), pp. 3396–3411.
- [8] Jingyi Fu, Benoit Perthame, and Min Tang. “Fokker–Plank system for movement of micro-organism population in confined environment”. In: *Journal of Statistical Physics* 184.1 (2021), p. 1.